Sen, A., Cesca, S., Bishoff, M., Meier, T., Dahm, T. (2013): Automated full moment tensor inversion of coal mining induced seismicity. - Geophysical Journal International, 195, 2, pp. 1267—1281.

DOI: http://doi.org/10.1093/gji/ggt300

Geophysical Journal International

Geophys. J. Int. (2013) **195,** 1267–1281
Advance Access publication 2013 August 30

doi: 10.1093/gji/ggt300

Automated full moment tensor inversion of coal mining-induced seismicity

Ali Tolga Sen,[1] Simone Cesca,[1,2] Monika Bischoff,[3] Thomas Meier[4] and Torsten Dahm[2]

[1] *Institute of Earth and Environmental Science, University of Potsdam, D-*14476 *Potsdam, Germany. E-mail: tolgasen@geo.uni-potsdam.de*
[2] *Section* 2.1, *GFZ Potsdam, D-*14473 *Potsdam, Germany*
[3] *BGR, LBEG/NED, D-*30655 *Hannover, Germany*
[4] *Institute of Geosciences, Christian-Albrechts-University Kiel, D-*24118 *Kiel, Germany*

Accepted 2013 July 22. Received 2013 July 19; in original form 2013 March 26

SUMMARY

Seismicity induced by coal mining in the Ruhr region, Germany, has been monitored continuously over the last 25 yr. In 2006, a dense temporary network (HAMNET) was deployed to locally monitor seismicity induced by longwall mining close to the town of Hamm. Between 2006 July and 2007 July, more than 7000 events with magnitudes M_L from −1.7 to 2.0 were detected. The spatiotemporal distribution of seismicity shows high correlation with the mining activity. In order to monitor rupture processes, we set up an automated source inversion routine and successfully perform double couple and full moment tensor (MT) inversions for more than 1000 events with magnitudes above M_L −0.5. The source inversion is based on a full waveform approach, both in the frequency and in the time domain, providing information about the centroid location, focal mechanism, scalar moment and full MT. Inversion results indicate a strong dominance of normal faulting focal mechanisms, with a steeper plane and a subhorizontal one. Fault planes are oriented parallel to the mining stopes. We classify the focal mechanisms based on their orientation and observe different frequency-magnitude distributions for families of events with different focal mechanisms; the overall frequency-magnitude distribution is not fitting the Gutenberg–Richter relation. Full MTs indicate that non-negligible opening tensile components accompanied normal faulting source mechanisms. Finally, extended source models are investigated for largest events. Results suggest that the rupture processes mostly occurred along the subvertical planes.

Key words: Geomechanics; Fracture and flow; Earthquake source observations; Seismicity and tectonics.

INTRODUCTION

In mining environment, it is extremely important to monitor the spatial and temporal evolution of rupture processes. The determination of focal mechanisms, scalar moment, centroid location and extended source parameters can provide valuable information to detect weakened regions and evaluate risks of further dangerous ruptures or changes in structural properties, such as hydraulic permeability. With respect to tectonic earthquakes, which are typically well described by shear failures, mining-induced events can show different kind of rupturing types. Hasegawa *et al.* (1989) proposed different possible failure types for mining-induced seismicity, including normal and thrust faulting, pillar burst, roof collapses and outburst. Mining blasts can also be performed during the mine exploitation. A moment tensor (MT) representation offers a general model to describe a point seismic source and can be used to model all mentioned rupture processes within such approximation. While seismic sources of natural seismicity are often modelled by means of constrained MT, forcing the isotropic [ISO; and in some cases the compensated linear vector dipole (CLVD)] term to be null, seismic sources in mining environments should be modelled by a full MT. Most of the discussed processes, in fact, present significant, or even dominant, non-double couple (DC) components, including ISO components. Several MT inversion approaches have been developed in the last decades and successfully applied to a variety of seismic sources and spatial scales. Different studies specifically investigated source inversion in mining environments in the past (e.g. Feignier & Young 1992; McGarr 1992a,b; Trifu *et al.* 2000; Vavryčuk 2001; Fletcher & McGarr 2005; Sileny & Milev 2006; Julia *et al.* 2009; Lizurek & Wiejacz 2011; Vavryčuk & Kühn 2012), including coal, copper, zinc and gold mines as well as underground laboratories. Full MT source inversions were either performed modelling first onset polarities, combining polarities, amplitudes and spectra of different bodywaves (Feignier & Young 1992; Trifu *et al.* 2000; Vavryčuk 2001; Lizurek & Wiejacz 2011) and fitting bodywaves or full waveforms in the time domain (McGarr 1992a,b; Fletcher & McGarr 2005; Sileny & Milev 2006; Trifu & Shumila 2010; Vavryčuk & Kühn 2012). Data were either provided by surface,

borehole and in-mine sensors, including accelerometers, geophones and broadband seismometers.

MT applications have been typically applied to learn about sources in order to reduced number of events in the mining environment. McGarr (1992a) studied seismic tremors in a South African gold mine and inverted ground motion data of 10 events ($1.9 < M < 3.3$) to investigate MT components and source characteristics of these events. Most events showed significant implosive components and normal shearing. Feigner & Young (1992) used accelerometer data to determine the focal mechanisms of 33 seismic events down to moment magnitude −3.2, 12 events showed tensile cracks, 6 mostly implosive sources and the remaining 15 events showed mainly shear components. Dahm *et al.* (1999), Dahm (2001) and Manthei *et al.* (2001) studied MT and rupture of acoustic emissions in salt mines at about 15 kHz, and found predominant DC mechanisms and rupture lengths of about 20 mm. Sileny & Milev (2008) inverted amplitudes of body waves for five events (M_w 2.5–2.7) in a gold mine; resulting focal mechanisms showed significant non-DC components, and in most cases this non-DC component values are related with pressure of single couple, which fit with the physical model of pillar bursts. Julia *et al.* (2009) studied 76 earthquakes (M_w range 0.5–2.6) and inverted P, SV and SH spectral amplitudes to obtain MT components; their results showed that principal stresses were generally negative, a result attributed to gravitational effects on mined-out areas. Limitation to more extensive applications were due to the quality of the data and signal-to-noise ratio, which reduce the inversion performance for small events, as well as because of the wave propagation modelling in strongly heterogeneous mining environments. These difficulties also limited the performance of automated MT inversion routines; attempts for automated source inversion have been discussed for synthetic data in Trifu *et al.* (2000), and further tested on a salt mine data set (Trifu & Shumila 2010).

Different features, which are characteristic of mining environments, may pose a strong limitation to any seismological approach to model and invert seismic waveforms. First of all, given the presence of strong heterogeneities (voids, galleries, and different mineralogical bodies), observed high-frequency waveforms may only be reproduced by accounting for wave propagation in 3-D (when not 4-D, given the time evolution of the environment) velocity models. Vavryčuk & Kühn (2012) performed a MT inversion adopting a 3-D velocity model and discussed the limitation of simplified models in reproducing first onset polarities, amplitudes and waveforms. Simplified (e.g. homogeneous or 1-D) velocity models can be adopted when fitting lowpass filtered seismograms, removing the higher frequencies which are affected by small-scale heterogeneities; this approach may be limited to larger events, because of poor signal-to-noise ratios at low frequencies. A second problem, is that mining regions are typically (seismically) noisy environments, and recordings may show a poor signal-to-noise ratio, especially for weaker events. Seismic noise often presents a significant temporal variation as a consequence of mining activities, which can affect the inversion performance. Rydelek & Sacks (1989) showed that the number of events detected is larger during day time, because of mining activities, but the number of detected small events is higher during night time, because of the absence of cultural noise and better performance of the inversion approach. Finally, because of the large number of induced events in mining environments, manual processing is not viable to evaluate the rupture processes of detected seismicity, and automated inversion procedures must be set up. We choose here to perform the source inversion in the frequency domain, fitting full wavefom amplitude spectra, instead of the more standard time domain inversion approach. Such approach proved to be more robust in presence of model simplification or structural mismodelling (Dahm *et al.* 2000; Cesca *et al.* 2006; Sileny & Milev 2008) and allows the use of slightly higher frequencies with respect to the time domain approach. The algorithms we use have been developed based on the Kiwi tools (Heimann 2011), and follow an inversion scheme similar to those successfully adopted by Cesca *et al.* (2010a, 2011) for the analysis of seismic sources at regional distances. In our approach, both the DC, full MT and kinematic source parameters can be retrieved.

The aim of this paper is to implement a robust automated source inversion algorithms and investigate earthquake rupture processes following coal mining, both by determining DC and full MT point source models. Since most earthquakes are caused by shear faulting, DC source models can be first discussed. However, since induced mine tremors can include tensile and ISO components, a full MT inversion is also performed. Finite source inversion is more challenging because of the very small magnitudes (down to M −0.5) and the requirement to fit high-frequency radiation with a simplified velocity model. Because of this reason, we limit the application of extended source inversion to about 130 biggest events. Finite source inversion can provide information on the rupture plane and other extended source parameters, such as the size of the rupture. Since different inversion steps may be affected by inaccurate modelling of waveform propagation, we test the inversion using different velocity models and stations configurations, and perform the inversion at different frequency ranges. We finally propose an automated inversion scheme, and successfully apply it to more than 1000 events.

MINING ACTIVITY AND SEISMIC DATA

Coal mining in the Ruhr region, North Rhine-Westphalia, Germany, has been performed for centuries since early 13th century. The coal deposit spreads between the Lippe and Ruhr river. Geologically, the region is characterized by the presence of different coal-bearing layers from the Upper Carboniferous period. The Carboniferous strata comprise sandstone and claystone layers with distributed coal seams. This structure has an overall thickness of approximately 6000 m. The coal seams reach the surface in a strip along the Ruhr river and dip downward from the river to the North. The thickness of the coal layers ranges up to few meters. It is thinner for deeper layers, it increases up to 3–4 per cent workable seam between the Witten and Bochum strata (approximately between 2000 and 4000 m depth) and then drop again in the younger, upper stratas of the Upper Carboniferious (Drozdzewski 1993; Coldewey & Semrau 1994) According to Coldewey & Semrau (1994), the total thickness of the carbon layers is approximately 70 m. However, the authors only considered the first 3000 m depth structure.

Induced seismicity in the Ruhr region has been monitored by the Ruhr University Bochum since 1983 (Bischoff *et al.* 2010a). In this paper, we focus on the investigation of induced seismicity following longwall coal mining in the Hamm Heringen region, which is located at the eastern edge of the Ruhr region (Fig. 1). The process of longwall consists in the repeated mining and removal of single slice of ore. The mining activity processed at depths between 700 and 1500 m below the free surface. The size of the slices removed by the longwall mining had dimensions up to 300 m in height and 1000 m in length. The thickness of the coal seams was about 2 m (Bischoff *et al.* 2010a). The stope advanced with an average velocity of about 100 m month^{-1}. The mining region is considered tectonically inactive and all seismicity is induced or triggered by

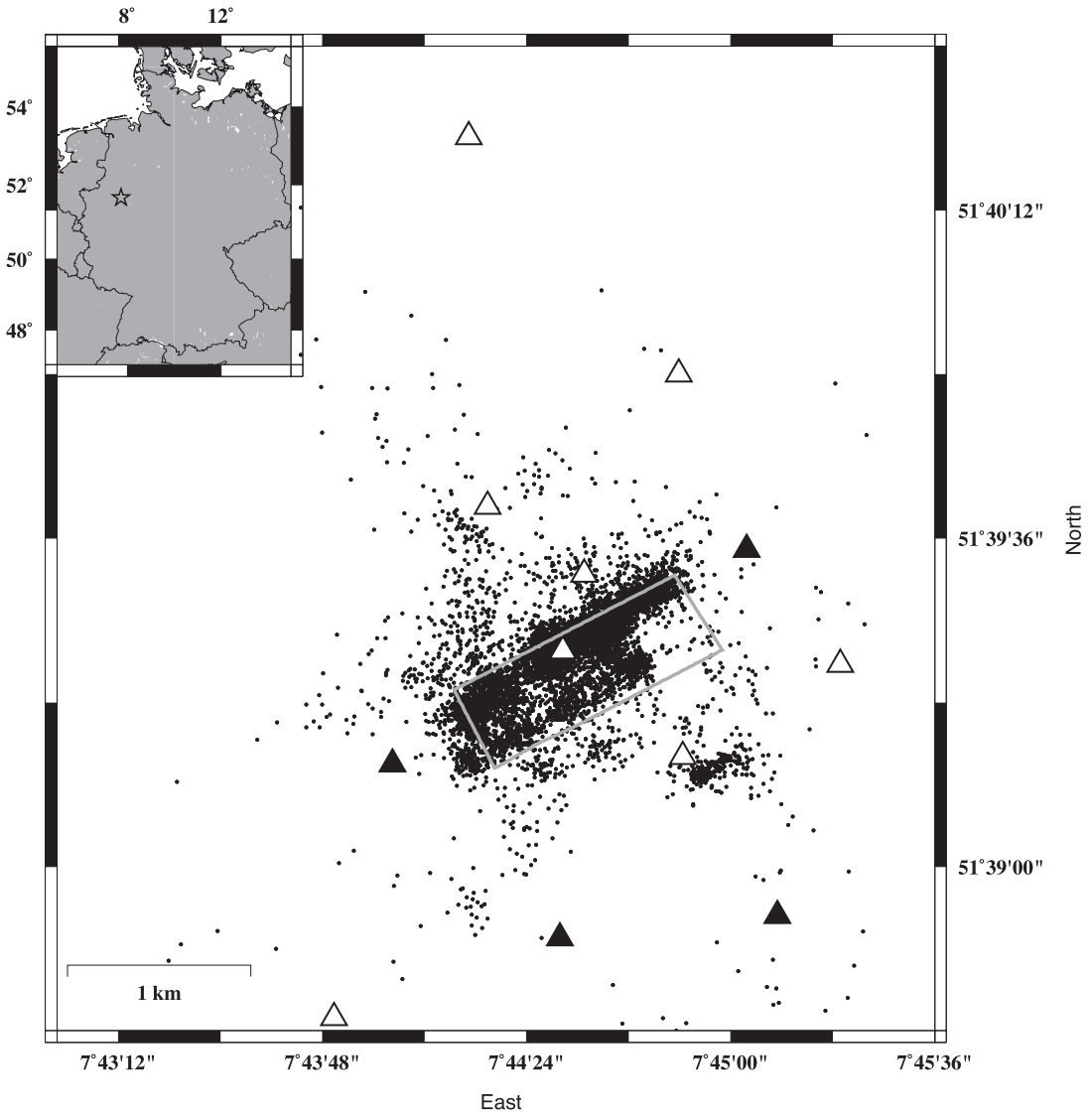

Figure 1. Geographical insight (left) and study region (right). White triangles denote short period stations and black triangles broadband stations. A grey rectangle indicates the geometry of the mined panel.

mining operations. The region close to the town of Hamm was continuously monitored by the HAMNET network, a local network running from 2006 June to 2007 July. Along the time of the network deployment, longwall mining was mostly performed between 2006 August and 2007 April. The network consists of 15 surface sensors: nine short-period (Mark L- 4C-3D, 1 Hz) and six broadband stations (five Güralp CMG, 60 s; one Trillium 40, 40 s). The network covers a region of about 2 km × 3.5 km (Fig. 1). Thanks to this local network, 7651 events could be detected and located during the monitoring interval (Bischoff *et al.* 2010a). However, about 5 per cent of these events have been related to mining activities at the neighbouring longwall in Bergkamen, and are therefore not discussed here. The remaining data set includes 7337 local events at the mining area (51.64–51.67 Lat N, 7.72–7.76 Lon E) in Hamm Heringen (Bischoff *et al.* 2010a). Epicentres are spread across a surface of 4 by 3 km, and about 90 per cent are located close to the longwall area. Hypocentral estimations (manual picking, based on P arrival time inversion) indicate source depths between 500 and 1500 m. The average source depth is at about 1000 m, which is approximately 100 m above the average mining level. Earthquake magnitudes range between M_L −1.7 and 2.0. The large number of events and the good quality of seismic waveforms provide an optimal data set to test the potential of automated MT and kinematic inversion routines for weak shallow induced events at a very local scale (below 2 km).

In this work, we initially consider all (more than 3000) events with magnitudes above or equal M_L −0.5. However, results will only be discussed for a subset of 1169 events, for which we obtain the most robust results (Fig. 2). The selection of best results has been based on a minimum number of observations and on the displacement spectra and time history misfits. The epicentral and depth distribution of the events used in this paper is shown in Fig. 2(a), where colour circles denote the spatiotemporal evolution of the seismicity: This shows a clear relation with the mining process, which proceeded from WSW toward ENE. The number of events increased during the mining activity and reduced again after the mining stopped. The frequency-magnitude distribution (FMD, Fig. 2b) does not follow the expected linear relation. Bimodal distributions have been often observed in mining environments (Kijko *et al.* 1987; Holub 1999). Possible explanations from the deviation to the Gutenberg–Richter

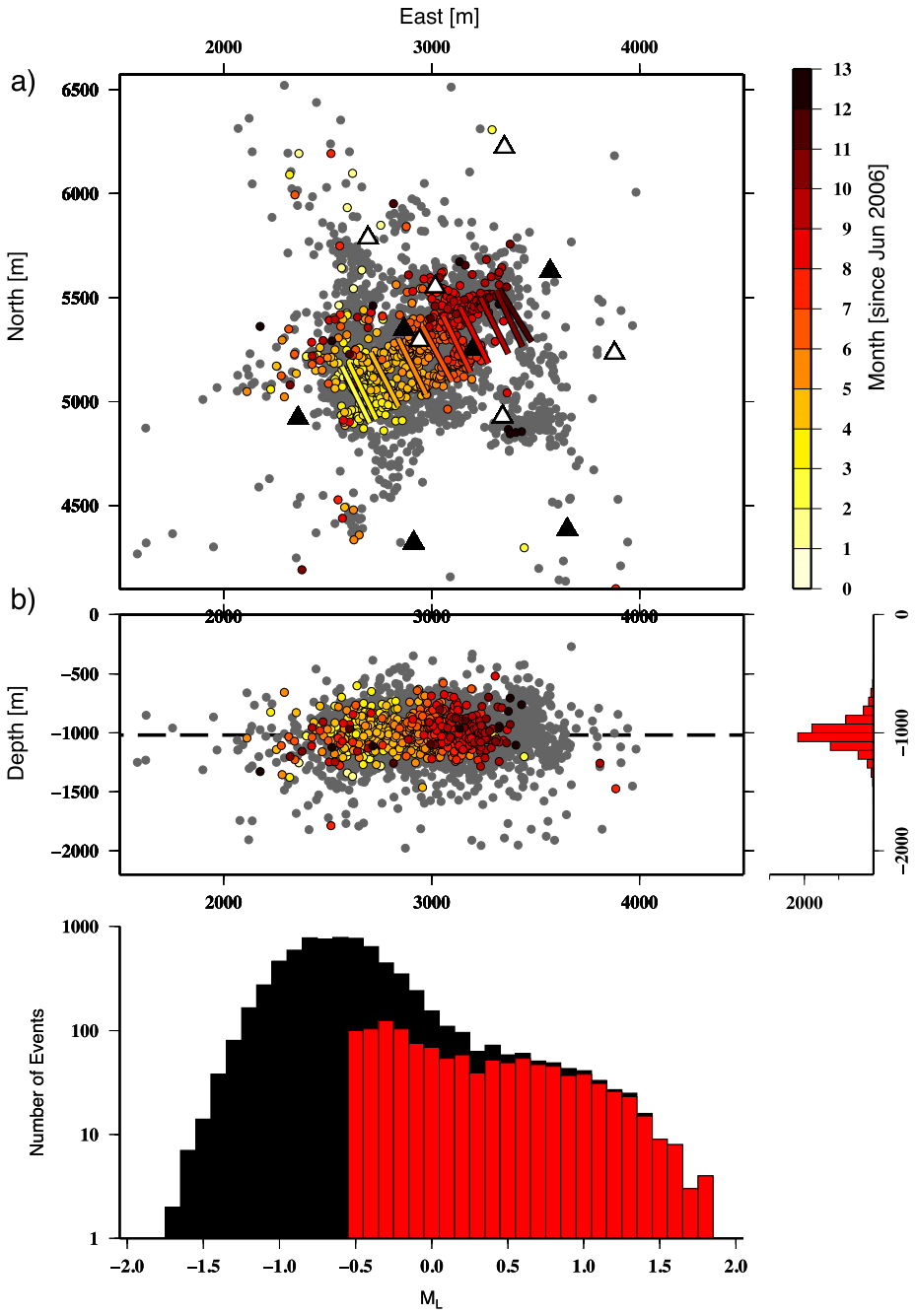

Figure 2. (a) Spatial distribution of all located events (grey circles), spatiotemporal distribution of events studied in this work (M_L larger/equal than −0.5, colour from yellow to red according to the timescale) and temporal shift of the longwall mining stope (coloured bars). (b) The non-cumulative FMD (bottom) is plotted for all recorded events (black histograms); red histograms indicate events successfully inverted in this work.

relation might be a change in the sensitivity of the monitoring network or the superposition of separated processes with different size distributions (Mendecki 2012). According to Kijko *et al.* (1987), Gibowicz & Kijko (1994) and Mendecki (2012), two different hypothesis have been proposed to explain these separated processes: events can be classified in groups of different origin, either because of their occurrence in different structural bodies, or because of their relation with mining-induced or residual tectonic stresses. Both the rock heterogeneity and the stress distribution can affect the distribution and size of events, which is controlled by the size and distance between brittle or stressed patches, where sources can nucleate and stop. The superposition of different groups of events, each of them with a different magnitude-frequency distributions, leads to the observed bimodal distribution. In particular, it has been suggested that a concavity of the distribution, as observed for our data set, could be generated by high activity of low magnitude events induced by mining excavation, and larger events caused by failure along pre-existing geological faults (Mendecki 2012).

METHODOLOGY

For the implementation of an automated source inversion algorithm for the mining environment we adopt the Kiwi tools (Heimann

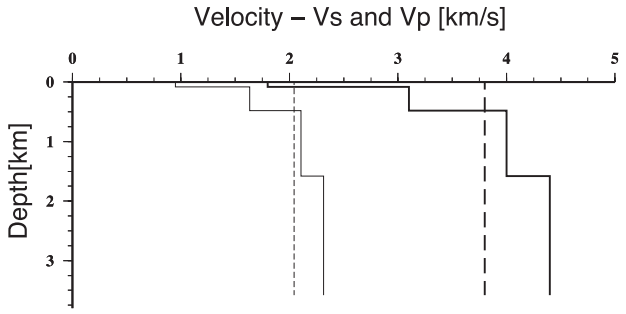

Figure 3. Layered (continuous lines) and homogeneous (dashed lines) velocity model used for the generation of Green's function (thick lines indicate vertical profiles for *Vs* and V_p, respectively).

2011). This software has been successfully applied to study seismic sources of moderate and large earthquakes at local and regional distances (Cesca *et al.* 2010b, 2012; Buforn *et al.* 2011; Custodio *et al.* 2012), and tested for automated routines (Domingues *et al.* 2012). However, they have never been routinely applied so far to small events in near-field distances with magnitude below M_w 3.5. The Kiwi tools allow synthetic seismograms generation and source inversions, both for DC, full MT and different kinematic models, and require pre-calculated Greens functions (GFs), which are stored in structured databases. We test here two possible velocity models: a homogeneous model ($V_p = 3.880\,\mathrm{km\,s^{-1}}$ and $V_s = 2.042\,\mathrm{km\,s^{-1}}$) and a layered one. This last model (Fig. 3) was defined according to Pelzing (1978), and is based on sonic logs from five boreholes, seismic reflection and geological profiles from the region. GFs have been generated using a reflectivity method [QSEIS code (Wang 1999)].

The inversion is performed at different steps, which are illustrated in Fig. 4 for a synthetic data set. In this example, data were generated with the layered model, while the inversion was performed assuming the homogeneous model. Note that, although 45 spectra and traces from 15 stations are fitted, only a small selection is shown for simplicity. The first point source inversion relies on the information available through the seismic catalogue compiled by the Ruhr University Bochum, which provide the hypocentral location and a first magnitude estimation. This information is used to set up a set of more than 10 000 starting configurations of the point source parameters (strike, dip, rake, moment and depth; e.g. we assumed 15 possible starting depths, in the range ±200 m with respect to the hypocentre location). In the first inversion step, we assume a DC point source model and perform the inversion in the frequency domain by fitting amplitude spectra of the whole trace. Since the inversion is non linear, we repeat the inversion iteratively for all considered starting configurations. A Levenberg-Marquardt approach is used to minimize the L2 norm misfit from each starting source model. As a result of this first inversion step, the fault plane angles (strike, dip, rake; four configurations due to intrinsic fault-auxiliary plane and focal mechanism polarity ambiguities), the centroid depth, the scalar moment and thus the magnitude. The fit of amplitude spectra is here preferred for the inversion, because it does not require a precise alignment of observed and synthetic waveforms, and because it is less dependent on the chosen velocity model. We use non-rotated displacement traces (North, East, vertical components), in order to keep spare horizontal traces, whenever a single trace is damaged or unavailable. Data and synthetics are tapered in the time domain (we use 8 s long time windows and apply a taper which smooths 1 s at both window sides) and a bandpass filter is applied in the frequency domain. After testing different frequency ranges (see discussion in the following text), three preferred bandpasses were chosen: 0.5–2, 1–3 and 1–4 Hz. Inversions were repeated for all these three bandpasses. Results of the amplitude spectra inversions are ambiguous, because compression and dilatation quadrants cannot be distinguished. The best DC model, as well as other possible non-DC models (e.g. a pure ISO source as well as dipole and tensile cracks with different orientations), are chosen as starting models for the following amplitude spectra inversion step, where a full MT point source model is assumed. Tapering, bandpass filtering and inversion approaches remain unchanged, so that the new misfit estimation can be directly compared with those of the DC model. The retrieved full MT is decomposed into DC, CLVD and ISO components using the MoPaD tool (Krieger & Heimann 2012). In the next inversion step, we determine the focal mechanism polarity, by computing synthetic displacement traces for both polarities with the observed waveforms. A grid search for possible centroid locations and centroid times, around the starting values (epicentre) is also performed. At the end of this stage, all point source parameters are derived (strike, dip, rake—two possible configurations, depth, moment and centroid coordinates). As a last step, a kinematic source inversion may be carried out. We generally adopt a circular source model; the performance of alternative line source models is mentioned in the discussion section. Other, more complex fault model have been proposed for mines (e.g. Ortlepp sources, Mendecki & Lötter 2011). We choose here to use simplified finite source models, which are described by fewer parameters, to avoid any over parametrization of the inversion problem. For the finite source inversion we adopt the centroid location, focal mechanism and scalar moment according to the point source inversion results, and test a range of possible extended source models: two possible fault plane orientations are defined according to the best DC point source, eight rupture sizes range between 10 m (here equivalent to a point source, given the spatial sampling of the Green's function database) and 350 m radius, and five possible rupture propagations (outward, and four unilateral ruptures in different directions). The inversion is performed again by fitting amplitude spectra (here the L1 norm is chosen) and repeated for two frequency ranges (1–10 and 1–20 Hz).

METHOD EVALUATION TESTS

This section is devoted to the description and discussion of a set of tests, both with synthetic and real data, with the purpose of evaluating the reliability and stability of the inversion results.

A first set of synthetic tests aimed to evaluate to what extent the adoption of simplified and/or improper velocity models could affect the inversion results. Synthetic data were generated using realistic source parameters, wave propagation and source-receiver geometry. Synthetic seismograms have been computed for a source located at 51.65266 Lon E and 7.74858 Lat N with depth 1.0 km, approximately at the centre of the observed-induced seismicity. We consider nine source mechanisms: three pure DC point source focal mechanisms (striking with 70, 160, 310°, dip 70°, rake −90°), three full MT point source mechanisms (including 50 per cent positive ISO component; DC components are the same as for the three pure DC synthetic events) and three extended source mechanisms (again same pure DC focal mechanisms, circular, subvertical rupture areas, with radius 50 m, rise time 0.05 s and rupture propagating unilaterally upward with a velocity of $1.4\,\mathrm{km\,s^{-1}}$, corresponding to 70 per cent of V_s at the source depth). The orientation of focal

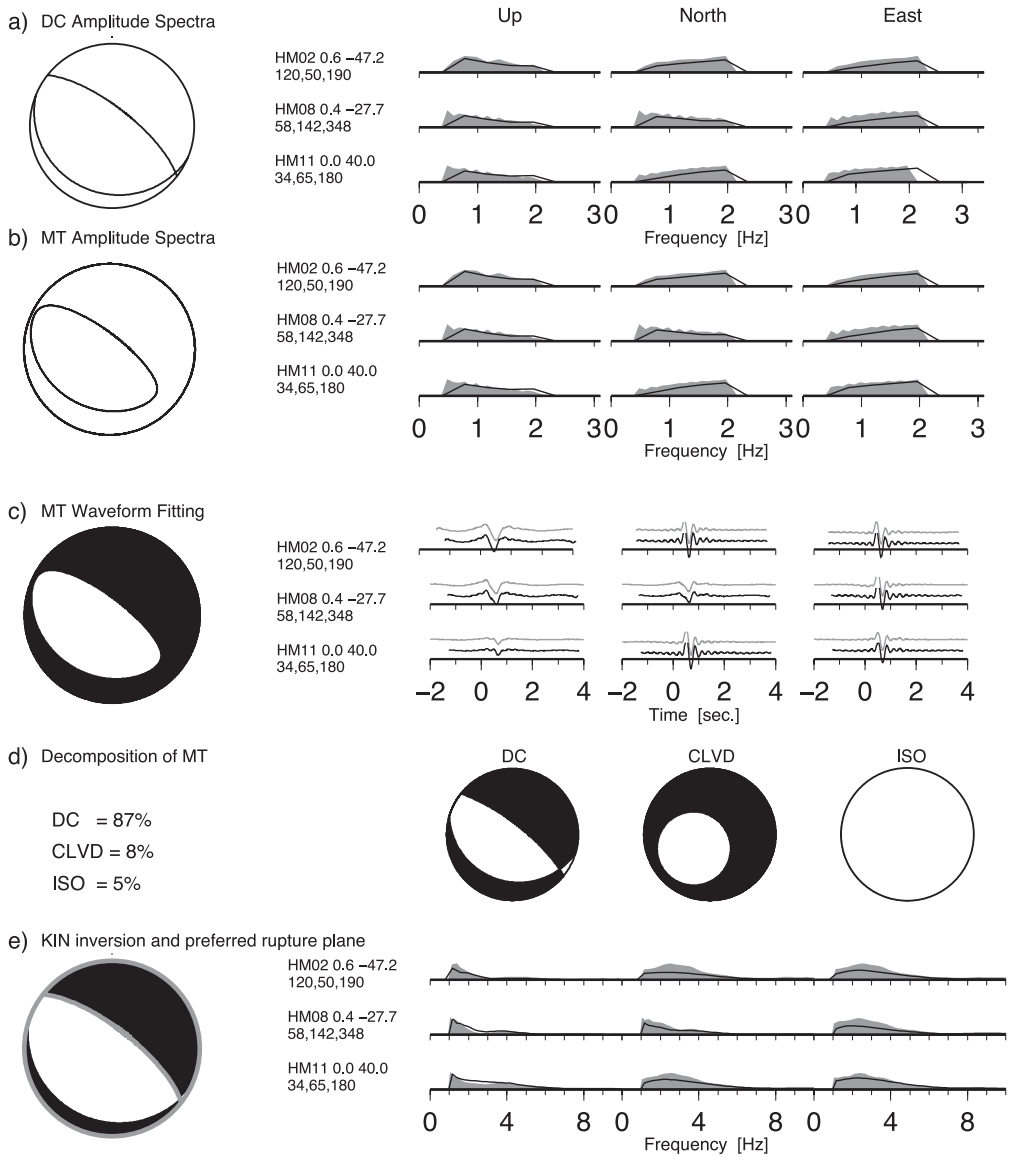

Figure 4. Example of the output of inversion process (synthetic event with M_w 1.1). (a) DC focal mechanism and fit of amplitude spectra (grey observed spectra, black synthetic spectra; selected stations only) after inversion step 1a. (b) Full MT focal mechanism and fit of amplitude spectra (grey observed spectra, black synthetic spectra) after inversion step 1b. (c) Full MT focal mechanism and fit of displacement waveforms (grey observed waveforms, black synthetic waveforms). (d) Percentage and focal sphere for the DC, CLVD and ISO components of the decomposed full MT. (e) DC focal mechanism and orientation of the preferred rupture plane (thick black line) and fit of amplitude spectra (grey observed spectra, black synthetic spectra) after inversion step 3 (kinematic inversion). All shown displacement traces and amplitude spectra are normalized.

mechanisms is consistent with the normal faulting derived by analysis of first motion polarities for selected events (Bischoff *et al.* 2010b) and with the results of our inversion, which will be discussed in the following section. All events have a magnitude M_w 1.6 (note that here the magnitude has no significant importance, and only affects waveforms amplitudes). Synthetic displacements are then computed with a sampling of 0.01 s at all HAMNET stations locations, both using the homogeneous and the layered velocity model. No noise has been originally included, since our aim here is to discuss the effects of waveform propagation mismodelling. The inversion is then performed for DC, full MT and kinematic models for all 18 data sets (nine source models and two velocity models), assuming both possible velocity models. Finally, we can discuss 36 inversion results, which are summarized in Fig. 5 (where DC, MT and kinematic inversion labels denote pure DC, full MT and finite source models used to generate the data).

All inversion results point out the reliability of the derived focal mechanism solutions: strike, dip and rake are well-retrieved even when non-DC components are present, when the source ruptured a finite region, and when a wrong velocity model is used to reproduce the data. The adoption of a wrong model only affects the misfit values, but not the determination of the correct point source model. Similar results are found for the inversion performed with full MT data: with all models we can correctly retrieve non-DC components. The adoption of a full MT source does not lead to the retrieval of anomalous finite source parameter: all kinematic

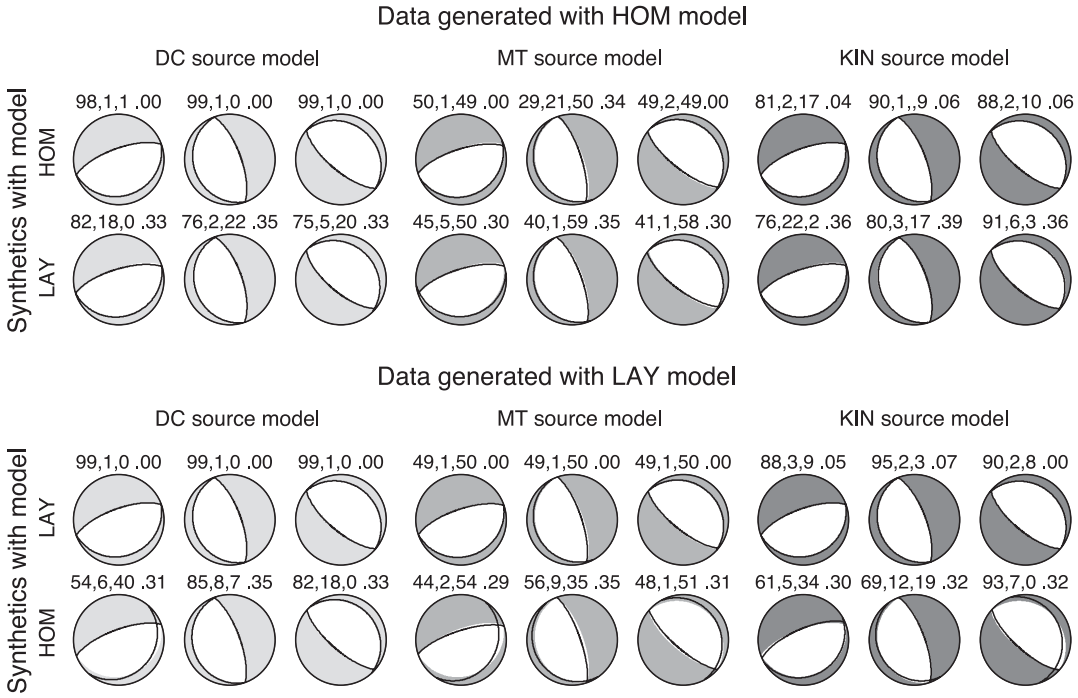

Figure 5. Synthetic tests for 3 different focal mechanisms (grey focal spheres) where the data generated for homogeneous (top) and layered (bottom) models; data are generated for pure DC sources (left), MT sources including 50 per cent positive ISO component (middle), and unilateral upward subvertical 50 m radius finite source models (right). Inversions are performed using the correct and wrong velocity models. Inversion results include the best DC model (thin black line focal mechanism), the decomposed MT (first three values above each focal mechanism indicate DC, CLVD and ISO component percentage). The last value given above the focal mechanism indicate the L2 norm misfit.

inversion performed with DC and MT source model indicate the smallest tested rupture radius (10 m), consistent with the point source models used to generate synthetic waveforms. Finally, inversions with data generated assuming finite source model indicated that: (a) DC source models are always well derived, even when using a wrong velocity model, (b) spurious non-DC components may be retrieved during point source inversion, up to 5 per cent CLVD, 14 per cent ISO and 17 per cent non-DC when using the correct velocity model, and up to 9 per cent CLVD, 24 per cent ISO and 27 per cent non-DC when using a wrong velocity model. The expected dominant DC components are always correctly derived. Rupture plane orientations, size and directivity are correctly retrieved when assuming the proper model, but can fail with a wrong one. Unilateral ruptures in other directions can be erroneously found and the rupture plane remain often poorly resolved, indicating that reliable finite source models require a realistic velocity model. Note, however, that we chose here a challenging setup, inverting for a vertical directivity using surface stations only. Unilateral ruptures along horizontal directions are better resolved with our station configuration. Finally, the inversion results point out that, likely because of the network geometry, we can better resolve finite rupture parameters for specific orientations of the rupture plane, with the best performance (better fit, low spurious non-DC terms, and correct results of the finite source inversion) for the source model with 70° strike. This suggests that the inversion performance may significantly change, depending on the focal mechanisms of different events. Repeating this synthetic events with noise contaminated synthetic seismograms (white noise, 10 per cent amplitude of the maximal amplitude) lead to increased non-DC anomalies, which can be as large as 20 per cent using the correct velocity model and 35 per cent when using the wrong one. The dominant DC components are always well resolved, as well as the orientation of the fault planes.

The second test was carried out using real data. Its main goal is to judge the stability of inversion results, which we discuss by following a jack-knife approach: we repeated each inversion test 15 times, each time removing one different stations, and discuss the distributions of retrieved source parameters, in comparison to best results, when the inversion is performed using all stations. A second goal is to discuss the reliability of the two chosen models, by discussing spectral fits of real data when computing synthetics for both velocity models. We choose a small data set: six events with variable magnitudes between M_L 0.5 and 1.8, for which reference solutions derived by using *P*-wave polarities and P-S amplitude ratios (Bischoff *et al.* 2010b) are available. The inversion is performed in the frequency range 1–4 Hz. Results are shown in Fig. 6. Even if retrieved focal mechanisms are often similar, independently on the chosen velocity model, synthetic spectra computed with a layered velocity model always provide a better fit. Therefore, for the following application to real data, we will only use the layered model. In most cases, DC inversion results are consistent with the reference polarity-based solutions. One exception is event 6, for which both our solutions consistently predict 5–10° striking mechanisms (for the steeper plane), different from the reference solution (strike −15°). A consistent focal mechanism for event 3 is only found for the layered model (using the homogeneous model we found an anomalous mechanism, but also obtain a very poor fit, indicator of the bad quality of the inversion result). The jack-knife test proof that results are very stable for most events, with the exception of event 3; the location of this event at the SW edge of the panel and the asymmetric stations distribution may be responsible for the observed instabilities, when removing some stations

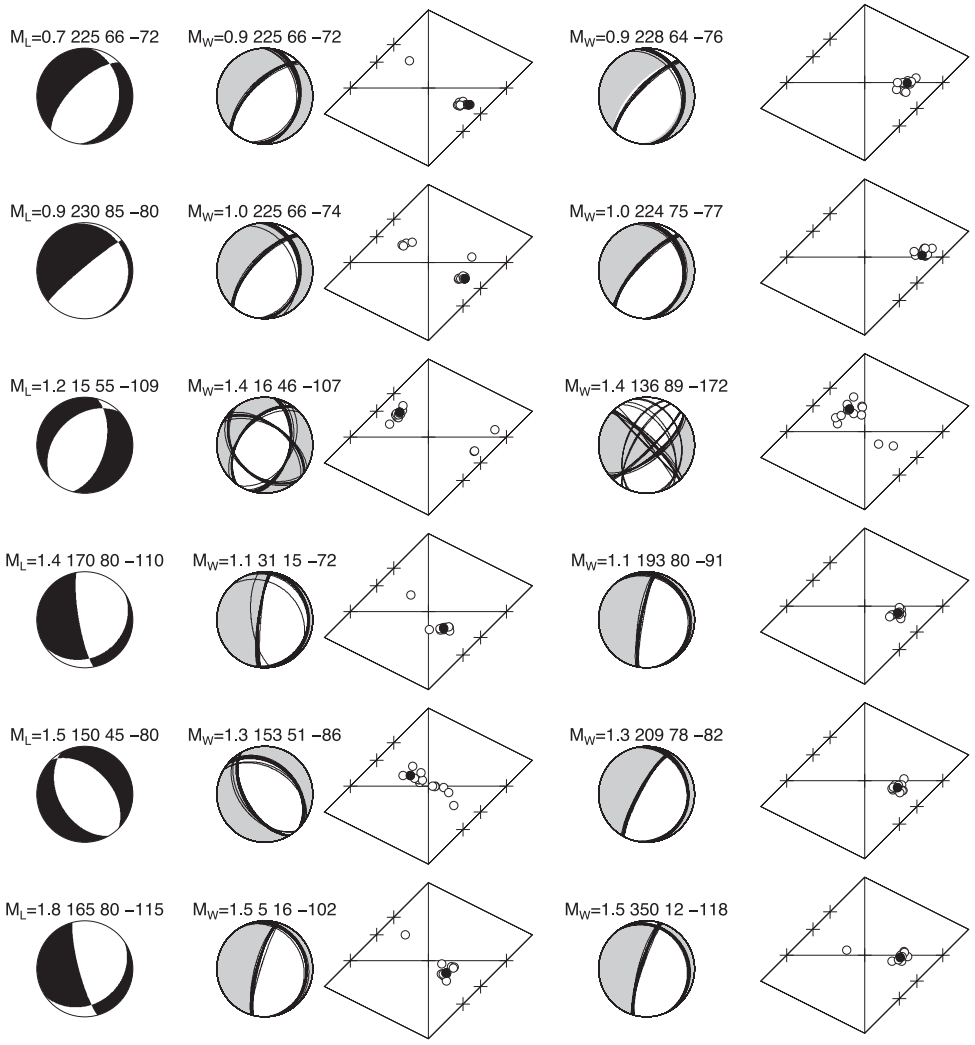

Figure 6. Focal mechanisms solutions based on first P onset polarities for six selected events (left, black focal spheres; magnitude, strike, dip and rake are reported above each focal mechanism) are compared with the results of our MT inversion (grey focal spheres; magnitude, strike, dip and rake are reported above each focal mechanism) using a layered (middle) and a homogeneous (right) velocity model. Thin black lines indicate all solutions obtained after the jackknife test. Full MT solutions are discussed using source type diagrams on the side of each solution (black circles denote best solutions, white circles results of the jackknife test).

from the full stations configuration. Full MT solutions generally show non-DC components. As expected, we find consistent signs of the CLVD and ISO components (solutions in the upper-left or lower-right quadrants). Non-DC component are comparable among inversion results with different velocity models. The jack-knife results are stable in terms of the amount of the non-DC terms, but in some cases their sign is not consistently retrieved, when removing some stations. In addition to these tests, we repeated the inversion of these six events using just broadband and short period stations separately. While amplitude spectra inversion has a similar performance and lead to comparable focal mechanism, time domain inversion indicate that waveform polarities are poorly resolved when using short period stations, where the waveform match become worse as misfit increase. The inversion using broadband stations only always provide solutions which correctly predicts the observed first onsets polarities. Because of these results the focal mechanism polarity (inversion step 2) will be based on the data from broadband stations only. The jack-knife test was also used to evaluate the uncertainties of single MT components, since it is well known that some components are poorly resolved in certain inversion conditions (for example, Mxz and Myz, when inverting low-frequency full waveform signals of shallow earthquakes). In our case, we found that on-trace components are worsely resolved, than off-trace components.

RESULTS

We apply the proposed inversion scheme to 3371 events, all events from the catalogue with magnitude above M_L −0.5). Fig. 7 shows an example amplitude spectra and waveform fits for a selected event (27.11.2006, $M_L = 0.7$). Results are only discussed for the best 1169 cases, which we consider the most reliable solutions. The selection of best solution was based on the inversion misfits (amplitude spectra misfits below 0.50, waveform misfits below 0.90; note that misfit in the time domain are strongly affected by noise and traces misalignment) and data quality (at least 12 traces available). Since more than 92 per cent of the focal mechanism has a

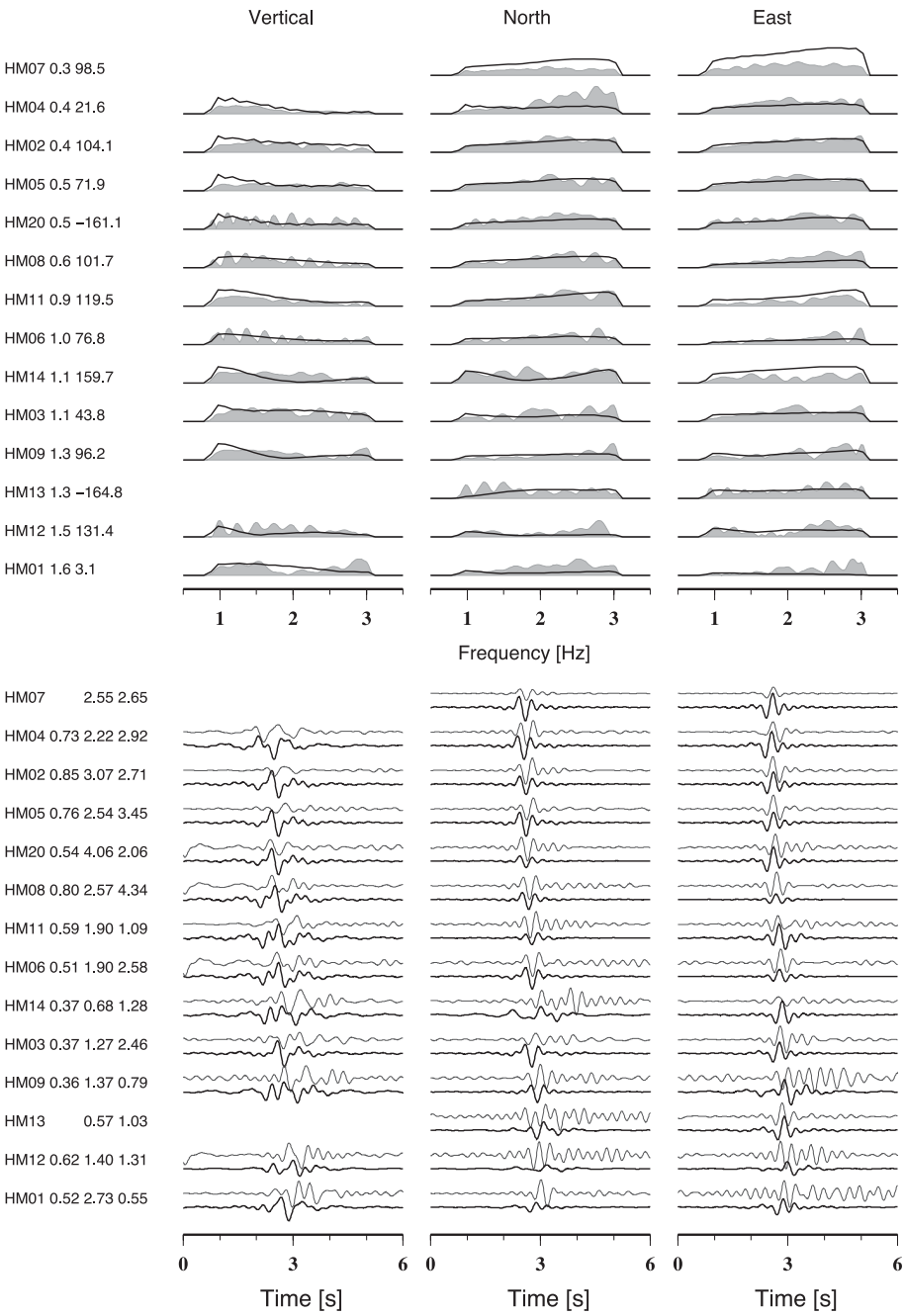

Figure 7. Spectra and waveform fit of a real event (2006 November 27 $M_L = 0.7$). Top: comparison of amplitude spectra of observed data (grey) and synthetics (black). Bottom: comparison of displacement seismograms of observed data (grey) and synthetics (black). Station names, distance (km) and azimuth (deg) are given on the upper left-hand side, station names and maximal amplitudes of plotted traces (in 10^{-6} m) on the bottom left-hand side. All shown displacement traces and amplitude spectra are normalized.

plane steeper than 45° and a second one shallower than 45°, we can discuss the distribution of fault plane angles (Fig. 8) for the planes with steeper dip angle only. Fig. 8 shows that most events have similar focal mechanisms, which can be classified in few classes upon their strike angle. Rake angles (Fig. 8a) show that most events occur as normal faulting (90 per cent of the events between $-110°$ and $-70°$, following Cronin 2004); the distribution is not symmetric and a relevant number of oblique events are found. The plot of the dip angle distribution (Fig. 8b), indicate that for most events the steeper plane is dipping between 50° and 65°. Finally, strike angles highlight different clusters of events, with strike angles of about 70°, 160°, 250° and 310°. This finding can be easier discussed in Fig. 9, where the number of events is plotted along strike-dip, strike-rake and dip-rake diagrams, where families of events with similar focal mechanisms can be better identified. The strike angles of the clusters are fitting with the orientation of the mining walls and stope, which are here indicated by dashed lines. Fig. 9, bottom, illustrate the temporal evolution of the spatial (Fig. 9b) and magnitude (Fig. 9c) distributions within each cluster. Specific patterns characterize different clusters, in terms of the temporal, spatial and magnitude distributions of seismic events. For example, clusters 1 and 4 are more localized in space and time: they almost occur at

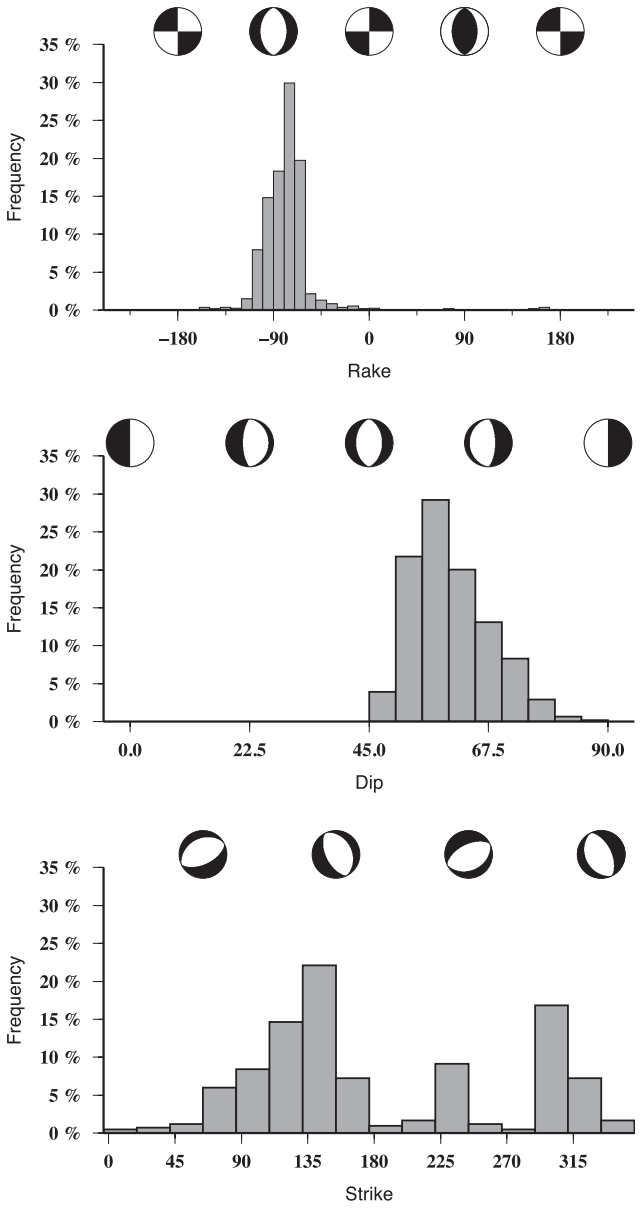

Figure 8. Distribution of DC solutions for fault plane angles for the steepest plane: rake (a), dip (b) and strike (c) distributions.

the beginning and end of the study period, and at the SW and NE edge of the panel, respectively. On the contrary, events of cluster 2 take place during the whole time frame and epicentres are spread in a larger region. Looking at the magnitude distribution (Fig. 9c), we can see that largest events, with M_w larger than 1 occur mostly within clusters 3 and 4.

Full MT inversion has been performed for the same data set (1169 events). To discuss full MT results, we perform its decomposition and plot DC, CLVD and ISO components on a source-type diagram (Hudson *et al.* 1989). Fig. 10 summarizes these results, showing the distribution of full MT mechanisms according to ISO, DC and CLVD percentage and source type plots (Fig. 10). For most events the DC component dominates the deviatoric term (DC is larger than CLVD). The distribution of CLVDs resemble the patterns observed also for natural events For example, see Cesca *et al.* (2012), who discussed the distribution of spurious CLVD terms resulting from the limitation of the modelling approach (e.g. because of noisy data or poor knowledge of the velocity model). This would at first suggest CLVD components are spurious terms, only retrieved because of an approximated description of the velocity model, or an unfavourable network geometry. However, the distributions of DC and ISO components provide a different image: most of the events show relevant ISO components, which can account for up to 50 per cent of the energy release. Note that for tectonic earthquakes, the ISO component is often significantly larger than values obtained in synthetic tests. The centre of the source-type plot is underpopulated, indicating few pure DC events, whereas most events are characterized by a combination of shear and tensile cracks. In most cases (more than 60 per cent), we observe opening cracks (combination of positive ISO and positive CLVD) rather than closing ones (negative ISO, negative CLVD, about 30 per cent). This clear predominance seems quite reliable, despite the polarity resolution problem highlighted by the jack-knife test. Only in few cases (less than 10 per cent), we have ambiguous ISO and CLVD signs.

From the spectral analysis performed for a random subset of events, with magnitudes ranging between M_w 1.0 and 1.8, corner frequencies were estimated approximatively between 3 and 15 Hz. Corner frequencies derived from S phase spectra for different magnitudes are slightly higher than those derived using *P* waves. Low corner frequencies (for the given magnitude range) and a low ratio between *P* and *S* waves corner frequencies suggest that the failures occur with a slow rupture velocity (Kwiatek *et al.* 2011), which could help the resolution of finite rupture parameters. Based on this findings, in the following kinematic inversion, we have chosen a rupture velocity of about 1.4 km s^{-1}, which is 0.7 times the *S*-wave velocity at the source depth, as estimated from the local layered velocity model (Fig. 3). Kinematic source model inversion was then carried out for 158 events, all events with $M_L \geq 1.0$ and with a reliable point source solution. When limiting the inversion to the lowest frequencies, below the corner frequency, extended source models cannot be investigated, and both point and kinematic source model fit equally well the observed amplitude spectra. For the range of considered magnitudes and the spectral analysis, the inversion with frequencies up to 10 and 20 Hz should have the potential to resolve finite source parameters, at least for largest events. However, in most cases (84 per cent for 1–10 Hz, 57 per cent for 1–20 Hz) the best finite source solutions have the smallest tested size, which make them equivalent to a point source (the discretized extended source model is composed by a single point source). For the remaining cases, when a larger size is found (in general a radius of 25 m), subvertical fault planes are preferred to subhorizontal ones. This result is found consistently for both frequency ranges: the subvertical planes are preferred in 64 per cent of the cases, for a bandpass 1–10 Hz, and in 81 per cent of the cases, when including frequencies up to 20 Hz. No clear directivity pattern is resolved. Finally, it should be noted that the estimation of the rupture sizes is strongly biased by the adoption of a given rupture velocity: in general, after testing the adoption of different rupture velocities, we observed a trade-off between rupture velocity and rupture radius, which makes difficult to discriminate between larger and faster source models, and smaller and slower ones.

DISCUSSION

The overall performance of the proposed point source inversion scheme indicates that our approach can be successfully used to automatically analyse large data sets in mining environments, and demonstrate the potential application of the Kiwi tools for local data sets and microseismicity data. Different from most source inversion

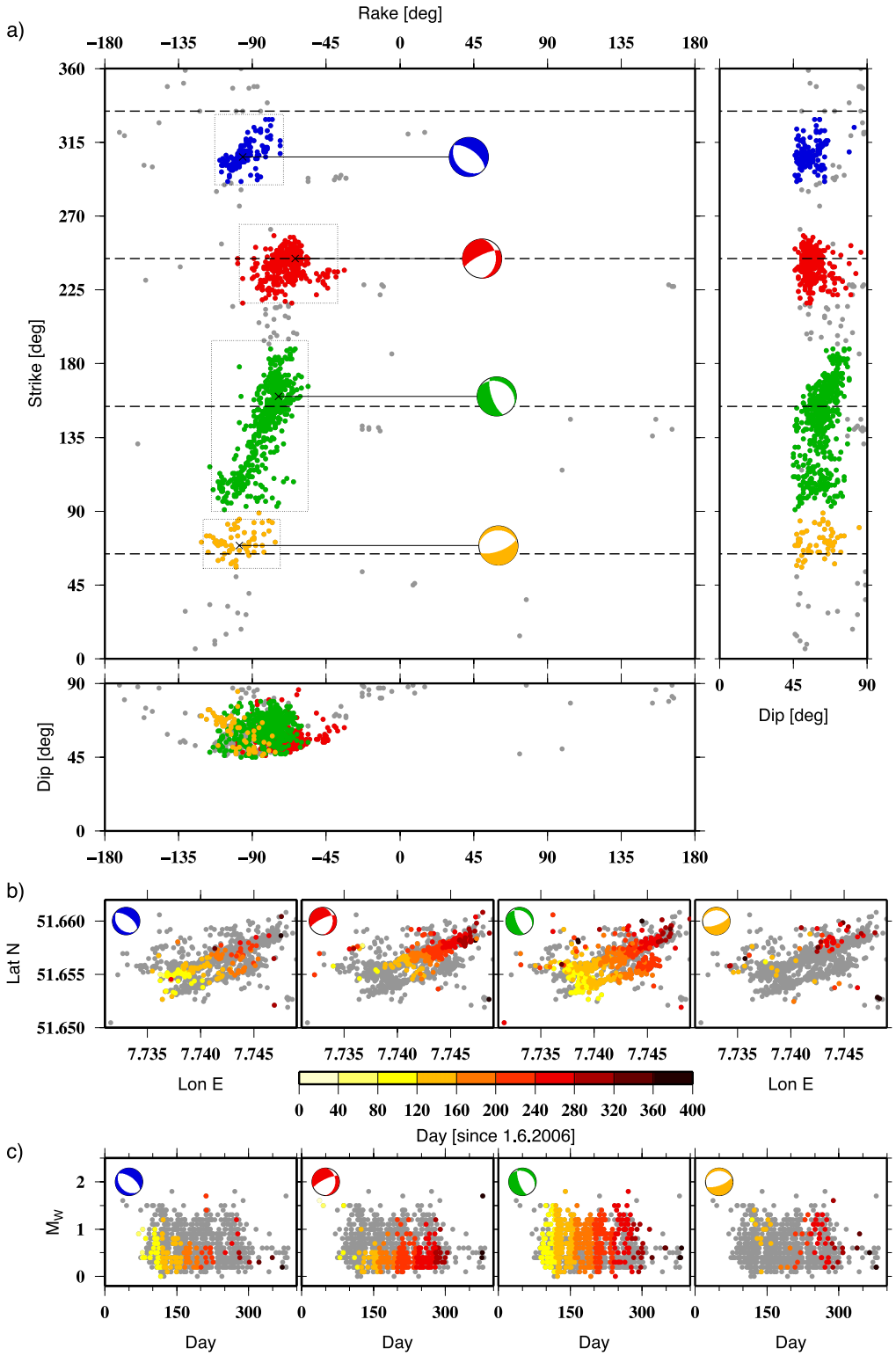

Figure 9. (a) The number of events along strike-rake, dip-rake and strike-dip plots highlights four clusters (dotted squares) of events with similar DC focal mechanisms (coloured focal spheres). Clusters show similar normal faulting, but different strike orientations, which are consistent with the orientation of mining walls (dashed lines). (b) Spatiotemporal distribution of the four clusters and (c) Temporal evolution of the magnitude distribution of the four clusters.

techniques typically adopted in mining monitoring, our method relies on the fit of the full waveform, rather than only on the body-wave polarities. The performance of the first inversion step in the frequency domain (amplitude spectra) allows us to ignore problems associated to waveform alignment and reduces the effects due to wave propagation mismodelling and the adoption of simplified layered models. The method performance may be limited in presence of strongly heterogeneous media, where the adoption of 1-D models

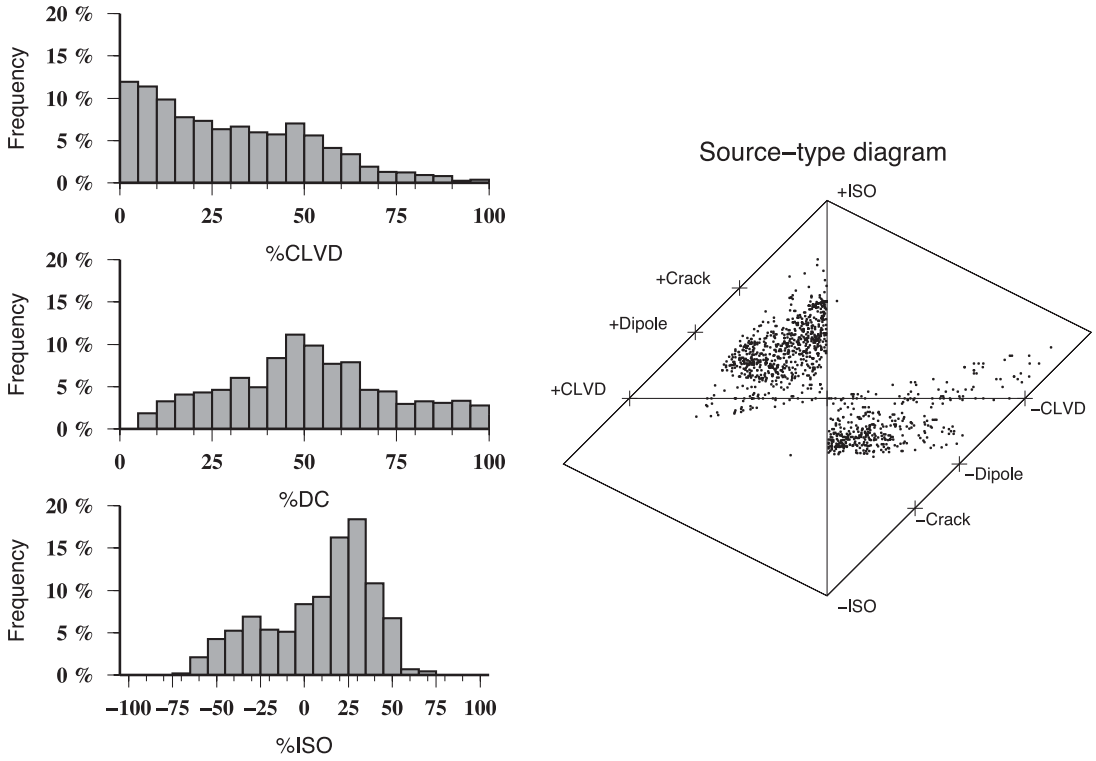

Figure 10. Left: distribution of decomposed terms (DC, CLVD, ISO) after full MT inversion. Right: source type plots are shown for each single event (black circles).

may be improper. Other cases where we expect a worse performance for mining environments includes the simultaneous occurrence of different events or the case of specific processes, such as rockfalls, where the energy is released over a longer time and with a complex source time function. The method has the potential to be extended to consider wave propagation in 3-D media, upon a reconfiguration of the Green function database. Another possible expansion, which should benefit the inversion stability, is the inclusion of surface and in-mine sensors, which would improve the coverage of the focal region.

The amount of inversion results make unfeasible a manual analysis of all event solutions, and some outliers in the MT catalogues cannot be excluded. Therefore, we chose here to discuss the best results and the average patterns of source parameters, when most events lead to similar results. This allowed us to draw general conclusions concerning the seismicity patterns. In this way, we could highlight that most events repeatedly occur with similar mechanisms, correlated with the mining geometry, and could define on this base few clusters of events. A similar approach was used to point out the presence of a significant non-DC components, indicating mostly positive tensile cracks in addition to shear crack. The reliability of these terms is supported by the fact that ISO and CLVD components generally have a consistent signs, and confirmed by the performance of synthetic data sets inversions. Finally, synthetic tests confirmed that spurious non-DC are also not artifact obtained in consequence of a point source approximation to finite source ruptures with specific rupture patterns (e.g. a repeated directivity or rupture plane orientation).

Finite source inversion on the available data set was a very challenging task, even when limited to the largest events. The fact that most preferred solutions are consistent with point sources or indicating small size ruptures (radii below 50 m) highlights the limitations of our resolution. These results indicate that synthetic seismograms, generated with 1-D models, are not able to reproduce observed high frequencies and the 1-D velocity model is not realistic enough to test frequency above 10 Hz. The adopted rupture velocity plays also a role in the estimation of rupture size, since fast larger ruptures and slow small ruptures produce similar waveforms and such source models may not be distinguished. Slow rupture processes are supported by the detection of seismic energy at low frequency and the estimations of spectra corner frequencies. Even though single finite source inversion may not be considered reliable, the overall analysis of finite source models point out some common patterns, such as the preference for subvertical faults, rather than the subhorizontal ones. Given the local stratigraphy, with presence of different seams and layers, Bischoff *et al.* (2010a) proposed that the brittle failure associated to induced events only occur within thin layers. We compare therefore two finite source inversions, using the features of the eikonal source model: in the first case, we use the unbounded circular-shaped model, and in the second case, we bound it above and below the centroid depth, within a depth thickness of 20 m, to reproduce the failure of thin subhorizontal layers. The geometry of the seismogenic layer leads to a range of source geometries within two extreme cases: a line source model, when the rupture plane is almost vertical, and a circular model, when the rupture plane is horizontal. Main results are illustrated in Fig. 11, when the results of eikonal and bounded eikonal source misfits are compared to the point source ones (for bandpasses 1–10 and 1–20 Hz). Although finite source models can better fit the spectra, the improvement is often minor and do not significantly perform better than point source models. The comparison of eikonal and bounded eikonal sources indicate a slight preference for unbounded (circular) source models, but again the differences among fits are minor.

According to Hedley & Wetmiller (1985), comminuted fracturing and faulting processes, also referred to as strain energy burst, is a common process affecting intact rocks in mines. Fracturing takes

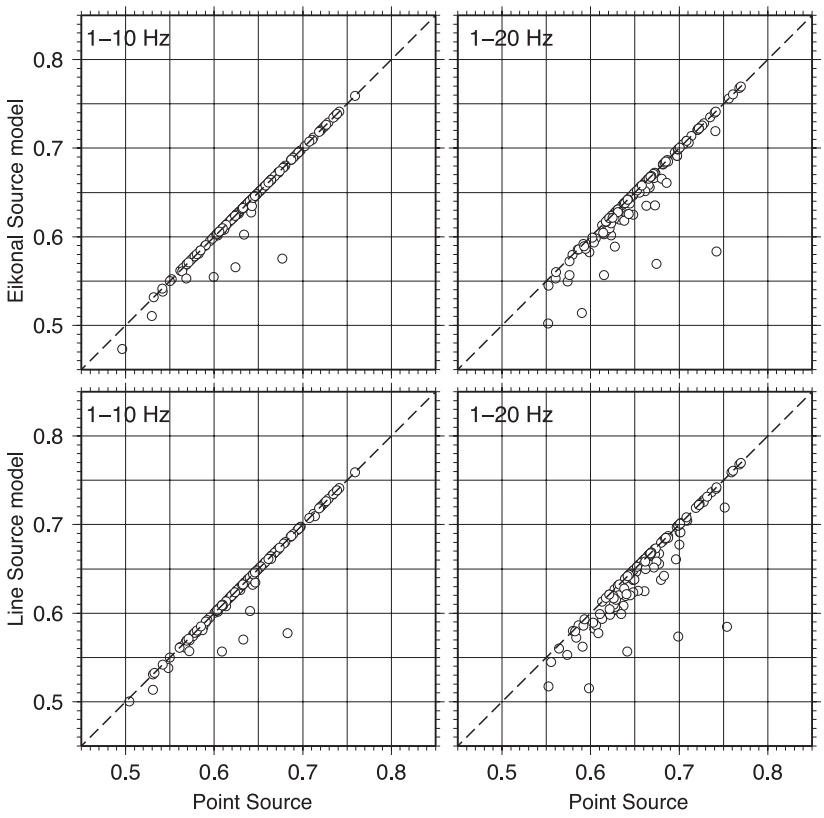

Figure 11. Top: misfit comparison among unbounded (circular) and bounded (line) eikonal finite source models inverted in the 1–10 Hz (left) and 1–20 Hz (right) frequency range. Bottom: misfit comparison among the bounded eikonal source model and the point source model in the 1–10 Hz (left) and 1–20 Hz (right) frequency range. Each point corresponds to an event. Dashed lines highlight equal misfits.

place as a normal fault, along subvertical planes in proximity of mine faces, and above the mining level. Comminuted faults are considered among the most common types of faulting in mines (Hasegawa *et al.* 1989). Our results, both in terms of source locations, focal mechanisms and preferred rupture plane geometry, suggest that this fracturing processes are also dominant in our study area.

Source model solutions can be classified into different clusters with similar source models, e.g. according to the orientation of the DC planes, the sign of the tensile crack component, or the determination of preferred kinematic solutions along the subhorizontal or subvertical plane. The availability of large focal mechanism data sets can be then used to investigate whether any of these source features can be related to the observed anomalous FMD and thus used to discuss its origin. FMDs are here discussed on the basis of M_w magnitude estimations, the outcome of our inversion, rather than on the original M_L values. Fig. 12 shows the cumulative and non-cumulative distribution from the entire data set (top) for which we obtain reliable solutions, as well as FMDs based on subsets (bottom), according to two classification approaches: in the first case subsets are based on the focal mechanism clusters derived in the analysis of DC point sources (see Fig. 9), in the second case based on the sign of the tensile component. Results from the first approach highlight different FMDs for different DC models. Clusters 1 (blue) and 2 (red) show a similar behaviour, following a Gutenberg-Richter distribution, with a completeness magnitude of about M_w 0.3. They include no events with magnitude above M_w 1.5. Events from clusters 3 and 4 (green and yellow circles) show an anomalous pattern, similar for both families of events, with a significant number of large events above M_w 1. The distributions do not fit the expected Gutenberg–Richter relation, unless considering an unrealistic high magnitude of completeness and low b-values, In general the superposition of two main families of events, clusters 1 and 2, and clusters 3 and 4, with different FMDs are responsible for the observed overall bimodal distribution of this coal mining-induced seismicity data set.

Our results are not sufficient to discriminate whether the overall FMD is only a consequence of structural heterogeneities or only a response to different acting stresses. The first hypothesis cannot be fully investigated, since large uncertainties on source locations limit the interpretation of the correlation between subsets locations and different structural bodies. The alternative hypothesis for the observed FMDs, based on the combined effects of tectonic and induced stresses, could fit to our findings, since focal mechanisms of different orientations have different likelihood to take place depending on the acting stresses. However, local stresses are poorly known, and therefore this hypothesis cannot be further assessed. The proposed approach for the focal mechanism classification and the following analysis of FMD for classes of subevents with a similar mechanism could be used in other environments (e.g. swarms, volcanoes), where deviation from the Gutenberg–Richter law is observed.

CONCLUSIONS

We propose an automated full waveform inversion approach, coupling amplitude spectra and displacement waveform inversion, to derive point and extended source models at very local distances, feasible for microseismicity and mining-induced seismicity analysis. After testing different stations configurations, velocity models and inversion parameters (e.g. frequency band), full waveform MT inversion was successfully applied to more than 1000 mining-induced events following longwall mining in a coal mine in Germany. Data

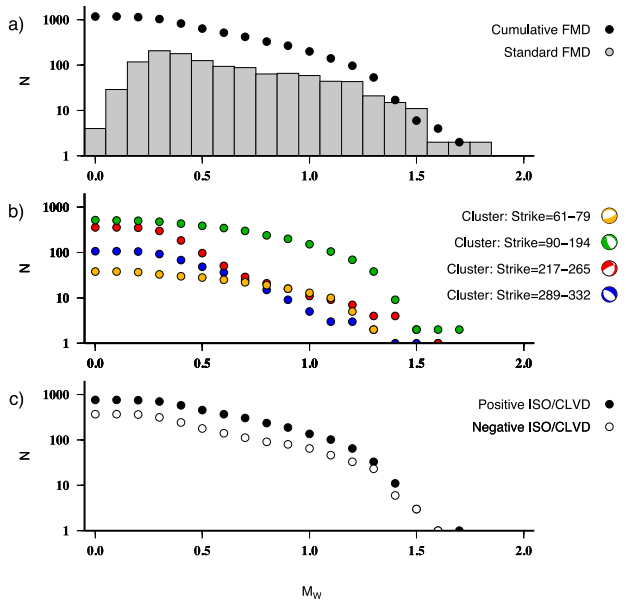

Figure 12. Overview of the FMD for different source classifications. (a) Cumulative (black dots) and standard (grey histograms) FMDs for the studied 1169 events. Bottom: cumulative FMDs after clustering the events respect to: (b) strike angle (colour dots according to the coloured focal mechanism, see also Fig. 6), (c) sign of the tensile/ ISO component (black dots for positive tensile/ ISO components, white dots for negative ones).

recorded at a local scale (<2 km) by a combination of broadband and short period stations, were used to derive source parameters for low magnitude events down to $M_L - 0.5$. The automated inversion process was applied to 3371 events and provided good spectral fit and reliable DC and full MT solutions for 1169 of them. Major conclusions can be summarized as follows:

- DC solutions are in good agreement with reference solutions, based on first polarities and *S* wave polarization, when available (about 100 events).
- A layered velocity model better reproduces observations than a simplified homogeneous model. Best results are obtained when fitting amplitude spectra and displacement traces in the range between 0.5 and 4 Hz.
- Focal mechanisms show similar style of faulting: a very large majority shows normal faulting, with one steep fault plane. Strike angles are parallel to the advancing mining stope or to the mining walls.
- Full MT inversion results shows that most of the events deviate from a pure DC model and include an opening crack component.
- Kinematic inversion results suggest that slow ruptures occur in most cases along the steeper fault. However, finite source parameters are poorly resolved.
- Events have been classified in different clusters according to their source parameters: the observed bimodal FMD is better explained by clustering the events according to their fault plane orientations.

ACKNOWLEDGEMENTS

We are thankful to the Ruhr University Bochum and to all researchers involved in the installation and handling of the local network, for monitoring and providing access to data used in this study. This work has been funded by the project MINE. The project MINE is part of the R&D-Programme GEOTECHNOLOGIEN, The MINE project is funded by the German Ministry of Education and Research (BMBF), Grant of project BMBF03G0737.

REFERENCES

Bischoff, M., Cete, A., Fritschen, R. & Meier, T., 2010a. Coal mining induced seismicity in the Ruhr Area, Germany, *Pure appl. Geophys.,* **167,** 63–75.

Bischoff, M., Fischer, L., Wehling-Benatelli, S., Fritschen, R., Meier, T. & Friederich, W., 2010b. Source mechanisms of mining induced seismic events in Hamm, Eastern Ruhr area, Germany, *ESC General Assembly*, Montpellier, France.

Buforn, E., Pro, C., Cesca, S., Udias, A. & Del Fresno, C., 2011. The 2010 Granada, Spain, deep earthquake, *Bull. seism. Soc. Am.,* **101,** 2418–2430.

Cesca, S., Burfon, E. & Dahm, T., 2006. Amplitude spectra moment tensor inversion of shallow earthquakes in Spain, *Geophys. J. Int.,* **166,** 839–854.

Cesca, S., Heimann, H. & Dahm, T., 2010b. Rapid directivity detection by azimuthal amplitude spectra inversion, *J. Seismol.,* **15,** 147–164.

Cesca, S., Rohr, A. & Dahm, T., 2012. Discrimination of induced seismicity by full moment tensor inversion and decomposition, *J. Seismol.,* **17,** 147–163.

Cesca, S., Dahm, T., Juretzek, C. & Kühn, D., 2011. Rupture process of the 7 May 2001 Mw 4.2 Ekofisk induced earthquake, *Geophys. J. Int.,* **187**(1), 407–413.

Cesca, S., Heimann, S., Stammler, K. & Dahm, T., 2010a. Automated point and kinematic source inversion at regional distances, *J. geophys. Res.,* **115**(24), B06304, doi:10.1029/2009JB006450.

Coldewey, W.G. & Semrau, L., 1994. Mine water in the Ruhr Area (Federal Republic of Germany), in *Proceedings of 5th International Mine Water Congress*, Nottingham, pp. 613–629.

Cronin, V.S., 2004. A draft primer on focal mechanism solutions for geologists: teaching quantitative skills in the geosciences. Available at: http://serc.carleton.edu/files/NAGTWorkshops/structure04/Focal_mechanism_primer.pdf, last accessed 24 July 2010.

Custodio, S., Cesca, S. & Heimann, S., 2012. Application to the 2007 Mw 5.9 horseshoe abyssal plain, offshore SW Iberia, earthquake, *Bull. seism. Soc. Am.,* **102,** 361–376.

Dahm, T., 2001. Rupture dimensions and rupture processes of fluid-induced microcracks in salt rock, *J. Volc. Geotherm. Res.,* **109**(1–3), 149–162.

Dahm, T., Horalek, J. & Sileny, J., 2000. Comparison of moment tensor solutions for the January 1997 West Bohemia earthquake swarm, *Studia Geoph. et Geod.,* **44,** 233–250.

Dahm, T., Manthei, G. & Eisenblätter, J., 1999. Automated moment tensor inversion to estimate source mechanisms of hydraulically induced microseismicity in salt rock, *Tectonophysics,* **306**(1), 1–17.

Domingues, A., Custodio, S. & Cesca, S., 2012. Waveform inversion of small to moderate earthquakes located offshore Southwest Iberia, *Geophys. J. Int.,* **192**(1), 248–259.

Drozdzewski, G., 1993. The Ruhr coal basin (Germany): structural evolution of an autochthonous foreland basin, *Int. J. Coal Geol.,* **23,** 231–250.

Feignier, B. & Young, R.P., 1992. Moment tensor inversion of induced microseismic events: evidence of non-shear failures in the $-4<M<-2$ moment magnitude range, *Geophys. Res. Lett.,* **19**(14), 1503–1506.

Fletcher, J.B. & McGarr, A., 2005. Moment tensor inversion of ground motion from mining induced earthquakes, Trail mountain, Utah, *Bull. seism. Soc. Am.,* **5**(1), 48–57.

Gibowicz, S.J., 1990. The mechanism of seismic events induced by mining. Rockburst and seismicity in mines, in *Proceedings of the 2nd international Symposium on Rockburst and Seismicity in Mines,* Minneapolis. A.A. Balkema, pp. 3–27.

Gibowicz, S.J. & Kijko, A., 1994. *An introduction to mining seismology,* Academic Press, 314 pp.

Hasegawa, H.S., Wetmiller, R.J. & Gendzwill, D.J., 1989. Induced seismicity in mines in Canada—an overview, *Pure appl. Geophys.,* **129,** 423–453.

Hedley, D.G.F. & Wetmiller, R.J., 1985. Rockburst in Ontario mines during 1984, CANMET, Energy, Mines and Recources Canada Report No. SP 85-5, 36 pp.

Heimann, S., 2011. A robust method to estimate kinematic earthquake source parameters, *PhD thesis,* University of Hamburg.

Holub, K., 1999. Changes in the frequency-energy distribution of seismic events during mining in the Ostrava-Karvina Coal Field, *Studia Geophysica et Geodaetica,* **43**(2), 147–162.

Hudson, J.A., Pearce, R.G. & Rogers, R.M., 1989. Source type plot for inversion of the moment tensor, *J. geophys. Res.,* **94**(B1), 765–774.

Julia, J., Nyblade, A.A., Durrheim, R., Linzer, L., Gok, R., Dirks, P. & Walter, W., 2009. Source mechanisms of mine-related seismicity, Savuka Mine, South Africa, *Bull. seism. Soc. Am.,* **99**(5), 2801–2814.

Julian, B.R., Miller, A.D. & Foulger, G.R., 1998. Non-double-couple earthquakes, *Rev. Geophys.,* **36,** 525–549.

Kijko, A., Drzezla, B. & Stankiewicz, T., 1987. Bimodal character of the distribution of extreme seismic events in Polish Mines, *Acta Geophys. Pol.,* **35**(2), 157–166.

Krieger, L. & Heimann, S., 2012. MoPaD—moment tensor plotting and decomposition: a tool for graphical and numerical analysis of seismic moment tensors, *Seismol. Res. Lett.,* **83,** 589–595.

Kwiatek, G., Plenkers, K. & Dresen, G., 2011. Source parameters of picoseismicity recorded at Mponeng Deep Gold Mine, South Africa: implications for scaling relations, *Bull. seism. Soc. Am.,* **101**(6), 2592–2608.

Lizurek, G. & Wiejacz, P., 2011. Moment tensor solution and physical parameters of selected recent seismic events at rudna copper mine, in *Geophysics in Mining and Environmental Protection, Geoplanet: Earth and Planetary Sciences,* eds Idziak, A.F. & Dubiel, R., Springer, **2,** 11–17.

McGarr, A., 1992a. An implosive component in the seismic moment tensor of a mining-induced tremor, *Geophys. Res. Lett.,* **19**(15), 1579–1582.

McGarr, A., 1992b. Moment tensors of ten Witwatersrand mine tremors, *Pure appl. Geophys.,* **139,** 781–800.

Manthei, G., Eisenblätter, J. & Dahm, T., 2001. Moment tensor evaluation of acoustic emission sources in salt rock, *Construction and Building Material,* **15**(5–6), 297–309.

Mendecki, A.J. & Lötter, E.R., 2011. Modelling seismic hazard for mines, *Australian Earthquake Engineering Society 2011 Conference*, Barossa Valley, Australia.

Mendecki, A.J., 2012. Size distribution of seismic events in mines, *Australian Earthquake Engineering Society 2012 Conference*, Gold Coast, Queensland, Dec 7–9.

Pelzing, R., 1978. Untersuchungen zur Ortung von Herden seismicsher Ereignisse, dagestellt an Beispielen aus einem Stationsnetz im Ruhrbergbautgebiet, *PhD thesis,* Ruhr-University, Bochum.

Rydelek, P.A. & Sacks, I.S., 1989. Testing the completeness of earthquake catalogues and hypothesis of the self-similarity, *Nature,* **337,** 251–253.

Sileny, J. & Milev, A., 2006. Seismic moment tensor resolution on a local scale: simulated rockburst and mine-induced seismic events in the Kopanang Gold Mine, South Africa, *Pure appl. Geophys.,* **163,** 1495–1513.

Sileny, J. & Milev, A., 2008. Seismic source mechanism—source mechanism of mining induced seismic events—resolution of double couple and non double couple models, *Tectonophysics,* **456,** 3–15.

Trifu, C.I., Angus, D. & Shumila, V., 2000. A fast evaluation of the seismic moment tensor for induced seismicity, *Bull. seism. Soc. Am.,* **90,** 1521–1527.

Trifu, C.I. & Shumila, V., 2010. Microseismic monitoring of a controlled collapse in field II at Ocnele Mari, Romania, *Pure appl. Geophys.,* **167,** 27–42.

Wang, R., 1999. A simple orthonormalization method for stable and efficient computation of Green's functions, *Bull. seism. Soc. Am.,* **89,** 733–741.

Vavryčuk, V., 2001. Inversion for parameters of tensile earthquakes, *J. geophys. Res.,* **106**(B8), 16 339–16 355.

Vavryčuk, V. & Kühn, D., 2012. Moment tensor inversion of waveforms: a two-step time-frequency approach, *Geophys. J. Int.,* **190,** 1761–1776.